



HAL
open science

Adaptive quantization of local field potentials for wireless implants in freely moving animals: an open-source neural recording device

Dominique Martinez, Maxime Clément, Belkacem Messaoudi, Damien Gervasoni, Philippe Litaudon, Nathalie Buonviso

► To cite this version:

Dominique Martinez, Maxime Clément, Belkacem Messaoudi, Damien Gervasoni, Philippe Litaudon, et al.. Adaptive quantization of local field potentials for wireless implants in freely moving animals: an open-source neural recording device. *Journal of Neural Engineering*, 2018, Special Issue on Open Source Tools in Systems Neuroscience, 15 (2), pp.025001. 10.1088/1741-2552/aaa041 . hal-02104576

HAL Id: hal-02104576

<https://hal.science/hal-02104576v1>

Submitted on 25 Aug 2022

HAL is a multi-disciplinary open access archive for the deposit and dissemination of scientific research documents, whether they are published or not. The documents may come from teaching and research institutions in France or abroad, or from public or private research centers.

L'archive ouverte pluridisciplinaire **HAL**, est destinée au dépôt et à la diffusion de documents scientifiques de niveau recherche, publiés ou non, émanant des établissements d'enseignement et de recherche français ou étrangers, des laboratoires publics ou privés.

Adaptive quantization of local field potentials for wireless implants in freely moving animals: an open-source neural recording device.

Dominique Martinez¹, Maxime Clément¹, Belkacem Messaoudi², Damien Gervasoni², Philippe Litaudon², Nathalie Buonviso²

¹ UMR7503, Laboratoire Lorrain de Recherche en Informatique et ses Applications (LORIA), Centre National de la Recherche Scientifique (CNRS), Vandœuvre-lès-Nancy, France

² Centre de Recherche en Neurosciences de Lyon, CNRS UMR 5292, INSERM U1028, Université Claude Bernard Lyon 1, Lyon, France

E-mail: dominique.martinez@loria.fr

Abstract

Objective. Modern neuroscience research asks for electrophysiological recording of local field potentials (LFPs) in moving animals. Wireless transmission has the advantage of removing the wires between the animal and the recording equipment but is hampered by the large amount of data to be sent at a relatively high rate. *Approach.* To reduce transmission bandwidth, we propose an encoder/decoder scheme based on adaptive non-uniform quantization. Our algorithm uses the current transmitted codeword to adapt the quantization intervals to changing statistics in LFP signals. It is thus backward adaptive and does not require sending side information. The computational complexity is low and similar at the encoder and decoder side. These features allow for real-time signal recovery and facilitate hardware implementation with low-cost commercial microcontrollers. *Main results.* As proof-of-concept, we developed an open-source Neural Recording Device called NeRD. The NeRD prototype digitally transmits 8 channels encoded at 10 kHz with 2 bits per sample. It occupies a volume of $2 \times 2 \times 2 \text{ cm}^3$ and weighs 8 grams with a small battery allowing for 2 hours 40 min of autonomy. The power dissipation is 59.4 mW for a communication range of 8 m and transmission losses below 0.1%. The small weight and low power consumption offers the possibility to mount the entire device on the head of rodents without resorting to separate head-stage and battery backpack. The NeRD prototype is validated in recording LFPs in freely moving rats at 2 bits per sample while maintaining an acceptable signal-to-noise ratio ($>30 \text{ dB}$) over a range of noisy channels. *Significance.* Adaptive quantization in neural implants allows for lower transmission bandwidths while retaining high signal fidelity and preserving fundamental frequencies in LFPs.

Keywords: Neurotechnology; Neurophysiology; Wireless transmission; Neural telemetry; Neural implants; Local field potential

1. INTRODUCTION

UNDERSTANDING the neural bases of natural behavior and of neurological disorders involving the motor system like Parkinson's disease implies recording individual neurons or local field potentials (LFPs) in moving animals. Usually this is accomplished via extracellular electrodes implanted in the brain and a tethered connection between the animal and the recording equipment. Although signal multiplexing methods can greatly reduce the number of wires, the tether may still affect the animal's movements. In contrast, a wireless transmission bypasses this limitation by entirely removing the wires. For obvious reasons of robustness to noise, most studies considered digital [1-5] rather than analog [6-8] transmission. Yet, the system requirements in terms of low-power consumption and high throughput, typically several Mbit/s (e.g. > 5 Mbit/s for 16 channels at 20 KHz sampling rate and 16 bits of resolution), are difficult to achieve simultaneously using standard protocols (e.g. Bluetooth is too slow and WIFI consumes too much energy).

To reduce transmission bandwidth, the approach usually adopted is to perform online detection of neural events followed by data compression of the spike waveform [11-12]. This way, only spike characteristics and spike times are transmitted [1, 9, 10]. Yet, such a compression throws away the signal between the spikes and may introduce permanent errors due to imperfections in the detection of neural events [13-15]. And last, but not least, this approach is not applicable to LFPs. This is a serious drawback as the LFP represents an increasingly important signal in neuroscience and medicine. It underlies neural processes and may indicate neurological disorders, e.g. Parkinson's disease produces prominent LFP oscillations at beta frequencies in the basal ganglia of animal models. Thus, there is a need to record LFPs in moving animals with reduced transmission bandwidth and low computational and energy overhead (keep in mind that the device has to be mounted on the animal's head).

Data acquisition of neural signals is traditionally done through uniform quantization. A uniform quantizer is optimum only if the probability density function (pdf) $p(x)$ of the input signal x is uniform. If not, the quantization intervals should be non-uniformly distributed so as to yield an optimum representation of the input pdf. Yet, a fixed non-uniform quantizer would not be optimum for any LFPs as the pdf is not known *a priori* and the LFP signal is non-stationary; that is, the pdf

changes over time. We can thus define our problem to that of adapting the quantization cells over time to changing statistics in the LFP. To this aim, we propose in this paper a backward adaptive algorithm. Our algorithm merely uses the current transmitted codeword to adapt the quantization intervals. This way, there is no need of sending side information. The computational complexity is low and similar at the encoder and decoder side. These features allow for real-time signal recovery and facilitate hardware implementation. As proof-of-concept, we developed an open-source Neural Recording Device called NeRD. The NeRD prototype was mounted on rats' head and validated in recording LFPs at low bitrates (2 bits per sample).

2. MATERIAL AND METHODS

2.1 Theory

Asymptotically optimum quantizer. A n -bit non-uniform quantizer is defined by an ordered set of boundary points $\{x_i\}$, $i = 1 \dots N - 1$, delimiting $N = 2^n$ disjoint quantization intervals $R_i = [x_{i-1}, x_i]$, $i = 1 \dots N$, with quantization range $x_0 \equiv a$ and $x_N \equiv b$. A minimum average error (MAE) quantizer is optimum if it minimizes r -th power distortion

$$D_r = \sum_i \int_{x_{i-1}}^{x_i} |x - y_i|^r p(x) dx \quad (1)$$

where the y_i 's are the reconstruction levels associated to the quantization intervals. The most commonly used powers are $r = 1$ (mean absolute error) [16] and $r = 2$ (mean squared error) [17]. In high resolution quantization (large N), the pdf is roughly constant over individual quantization cells and the reconstruction levels are the midpoints of the quantization intervals, that is, in cell i , $p(x) \approx P(x \in R_i) / \delta_i$ with $\delta_i = x_i - x_{i-1}$, and $y_i = (x_{i-1} + x_i) / 2$. Thus, we can approximate the distortion (1) by

$$D_r = \frac{1}{2^r (r + 1)} \sum_i P(x \in R_i) \times \delta_i^r \quad (2)$$

A necessary condition for minimizing (2) is that every quantization cell has an identical distortion contribution [18-19], that is, the so-called *equidistortion principle* written as

$$P(x \in R_i) \times \delta_i^r = P(x \in R_{i+1}) \times \delta_{i+1}^r, \forall i \quad (3)$$

Note that in the case $r = 0$, the quantizer has maximum output entropy (MOE)

$$P(x \in R_i) = 1/N, \forall i$$

It has been shown that MOE and MAE quantizers are approximately equivalent for a class of signal pdfs that includes the Gaussian distribution [20].

Backward adaptive quantizer. A way to handle nonstationary inputs is to adapt the quantization cells over time in such a way as to satisfy equation (3) or (4) depending on the design criterion, that is, MAE or MOE quantizer. The boundary points are updated at each sample according to $x_i \leftarrow x_i + \Delta x_i$, $i = 1 \dots N - 1$. In forward adaptation (Fig. 1A), the boundary points change as a function of the input signal so that $\Delta x_i = \eta f(x)$ with $\eta > 0$ the adaptation factor. This scheme suffers that an excessive amount of side information is required to transmit the updates to the decoder. On the contrary, backward adaptation does not require transmitting additional bits as the quantization intervals change with the quantized output (Fig. 1B). The transmitted codeword $\{1_{x \in R_i}\}$ ($1_{x \in R_i} = 1$ if $x \in R_i$ and 0 otherwise) is now used instead of the input to update the encoder/decoder pair. Backward adaptation writes

$$\Delta x_i = \eta f(\{1_{x \in R_i}\}) \quad (4)$$

An adaptation function for MAE quantizers aiming at minimizing r -th power distortion is given in [19] as

$$f(\{1_{x \in R_i}\}) = \sum_{j=i+1}^N \delta_j^r \frac{1_{x \in R_j}}{N-i} - \sum_{j=1}^i \delta_j^r \frac{1_{x \in R_j}}{i} \quad (5)$$

At convergence, we have on average that $E[f(\{1_{x \in R_i}\})] = 0$ with E the expected value. As $E[1_{x \in R_j}] \equiv P(x \in R_j)$, equation (5) satisfy the equidistortion principle (3). A simplest formulation is obtained for MOE quantizers [21-22]. With $r = 0$, equation (5) simplifies to

$$f(\{1_{x \in R_i}\}) = \frac{1_{x \geq x_i}}{N-i} - \frac{1_{x < x_i}}{i} \quad (6)$$

with $1_{x < x_i} \equiv \sum_{j=1}^i 1_{x \in R_j}$ and $1_{x \geq x_i} \equiv \sum_{j=i+1}^N 1_{x \in R_j}$. At convergence of Eq. (6), we have on average that $E[1_{R_j}] \equiv P(x \in R_j) = \frac{1}{N} \forall j$. The boundary adaptation rules (5) and (6) were thoroughly analyzed in [19] and [21,22]. Details are not reported here to lighten the description of the adaptive quantizer. Backward adaptation for MOE quantizers is primarily of interest for real-time implementation because the complexity of equation (6) is low and similar at the encoder and decoder

side. Nevertheless, the decoder may not adapt appropriately if the transmitted codeword is corrupted by channel noise. To avoid the resulting encoder/decoder mismatch to remain in the system we introduce a leakage or forgetting parameter β in Eq. (4) as

$$\Delta x_i = \eta f(\{1_{x \in R_i}\}) - \beta x_i \quad (7)$$

From (7), it is shown in [23] that an initial difference $d_0(x_i)$ between encoder and decoder vanishes in time as $(1 - \beta)^t d_0(x_i) \rightarrow 0$ when $0 < \beta < 1$ and $t \rightarrow \infty$.

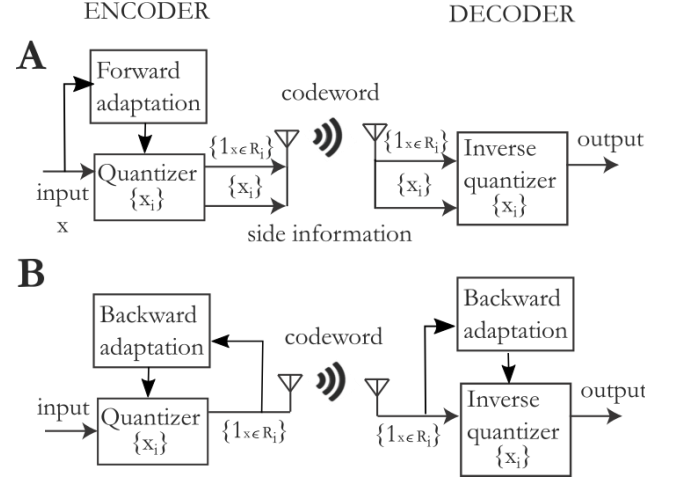


Fig. 1. Forward vs backward adaptation. The encoder/decoder pair is an adaptive non-uniform n -bit quantizer with a set of boundary points $\{x_i\}$. (A) Forward adaptation. The boundary points change as a function of the input. Side information is thus required to transmit the updates to the decoder. (B) Backward adaptation. The boundary points in the encoder/decoder pair change as a function of the transmitted codeword $\{1_{x \in R_i}\}$.

2.2 Open-source Neural Recording Device (NeRD)

We developed an open-source Neural Recording Device (NeRD) for real-time encoding/decoding of LFP signals. In NeRD, the quantizer operates on the difference between the LFP signal and a prediction (Fig. 2). The predictor is first-order (prediction coefficient $h = 1 - 2^{-4}$) and the quantizer is an adaptive MOE quantizer given by Eqs. (6) and (7) with adaptation factor $\eta = 200$ and leakage factor $\beta = 2^{-3}$. The use of parameters as negative powers of 2 greatly facilitates microcontroller implementation which can be done simply with shift operations. NeRD consists in two sub-systems: head-mounted emitter and base-station receiver (Fig. 3). The emitter is connected to eight electrode implants in the rat's brain (see section 2.3). For wireless transmission, the LFP

signal is quantized in a 2-bit format. The base-station receiver then decodes the received data stream to reconstruct the LFP waveform. Emitter and receiver are built from commercially available components. The schematics and firmware developed for NeRD are freely available at <https://github.com/pseudoincorrect>.

Head mounted emitter. The emitter is mounted on the rat's head and plugged to eight electrode implants via the nano-strip connector NSD-36-DD-GS from Omnetics. It occupies a volume of $2 \times 2 \times 2 \text{ cm}^3$ and weighs 4.5 grams (8 grams including a small battery LiPO 3.7 V 100 mAh). The battery life is approximately 2 hours 40 mins. The emitter consists of three stacked custom PCBs. The first stage is based on the electrophysiology chip RHD 2132 from Intantech Technologies. It performs signal acquisition and preprocessing; that is, $\times 192$ amplification and programmable filtering via a serial peripheral interface (SPI). In NeRD, the RHD was configured to record LFPs over 8 channels with 10 KHz sampling frequency, 0.1 Hz high-pass filter and 5 KHz low-pass filter. The second stage is based on the low-power microcontroller STM32F051C8T7 (32-bit ARM processor running at 48 MHz) from STMicroelectronics. It communicates with the RHD chip via the SPI port and runs an adaptive differential MOE quantizer. The LFP data are stored in a circular buffer before being quantized to $n = 2$ bits. Quantized data are then sent to the third stage which performs wireless transmission based on the low-power NRF24L01+ transceiver from Nordic Semiconductors. It offers a practical bandwidth of 1.34 Mbps, with selectable frequencies in the 2.4 GHz ISM band, for a power consumption of 11.3 mA at 3.0 V. The LFP waveforms are transmitted wireless as a stream of packets, each one containing the data (4 samples per channel over 8 channels) plus an overhead inherent to the Nordic transmission protocol (preamble, receiver address and cyclic redundancy check CRC).

Base station receiver. The receiver decodes the incoming packets by adapting the inverse quantizer and reformats the reconstructed signal as standard audio stream to facilitate interfacing with a PC via the USB port [5]. The USB audio protocol allows us to record and display the signals with existing audio editor software like Audacity. Without any power consumption restrictions at the decoder side, we selected a more powerful microcontroller with USB communication; that is, the STM32F411VET6U (32-bit ARM processor running at 100 MHz) from STMicroelectronics. Having a clock speed at the receiver higher than the one at the emitter allows us to control more peripherals. Hence, two

amplified transceiver modules are used in parallel to increase robustness against channel noise and packet loss, as in [5]. Whenever a failure is detected by CRC in one transceiver, the packet can still be recovered by redundancy at the other transceiver. The base station receiver also contains a digital-to-analog converter (DAC 8568 from Texas Instruments) to provide 8 analog output channels allowing electrophysiologists to use their own recording equipment by interfacing with a DB37 connector.

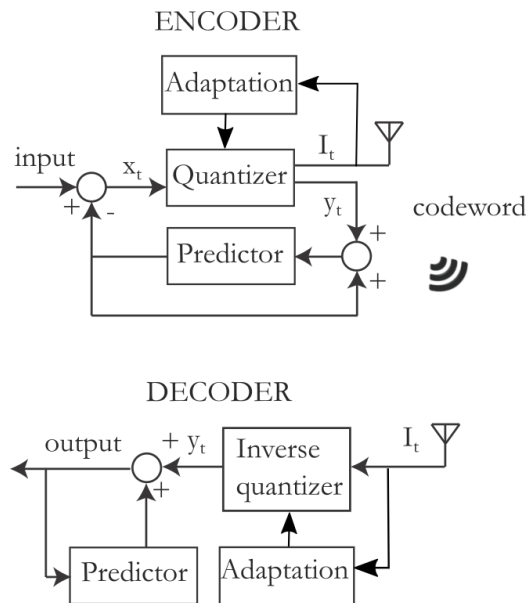


Fig. 2. Adaptive differential quantization in NeRD. The difference between the signal amplitude and a predicted value is quantized. In NeRD, the predictor is first-order (prediction coefficient $h = 1 - 2^{-4}$) and the encoder/decoder pair is a 2-bit adaptive MOE quantizer (Eqs. 6 and 7 with $\eta = 200$ and $\beta = 2^{-3}$).

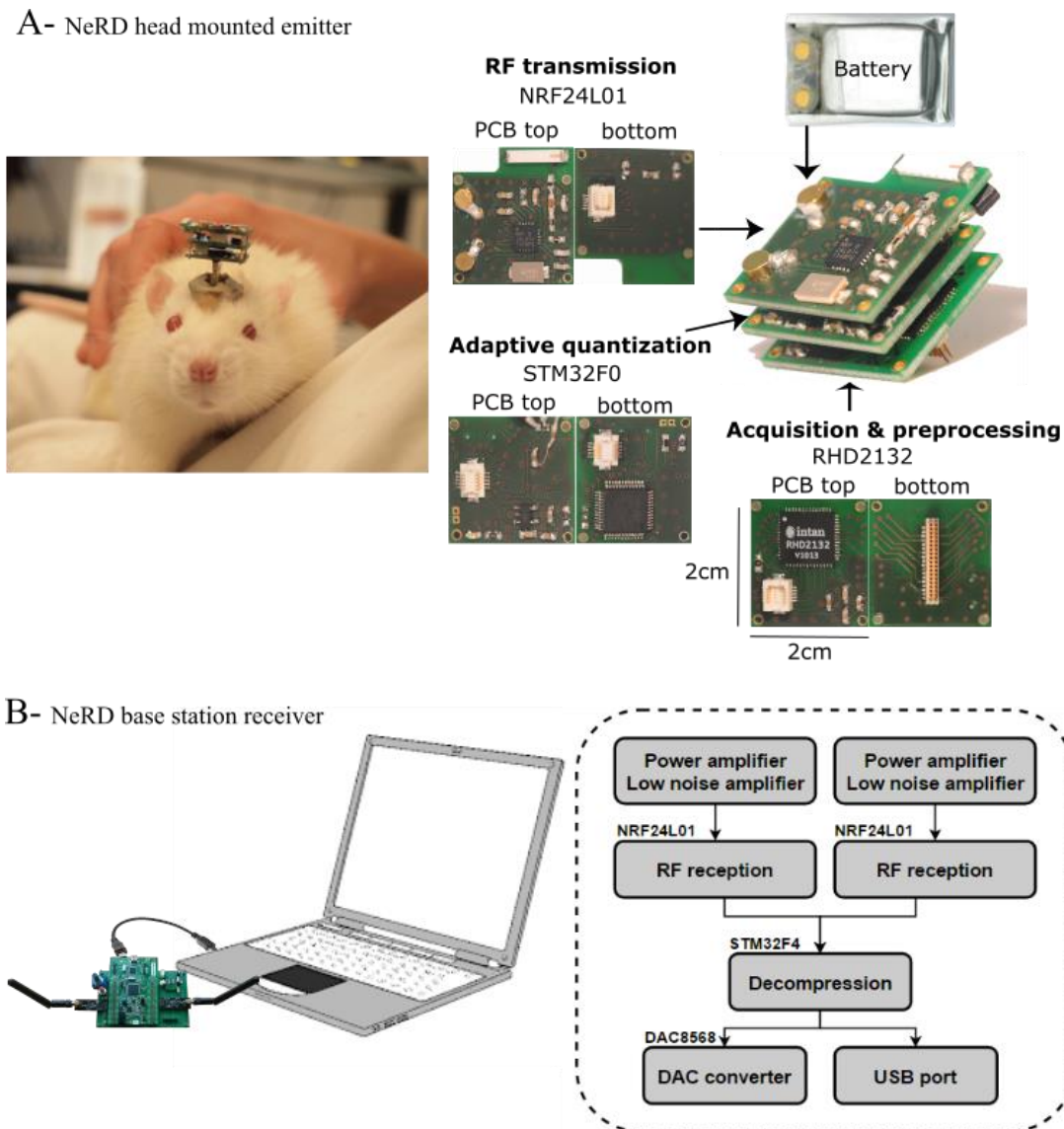


Fig. 3. NeRD hardware development. The system is open source and built from commercially available components. (A) Head mounted emitter. The emitter uses electrophysiology chip RHD2132 (Intantech), microcontroller STM32F0 (STMicroelectronics) and transceiver NRF24L01+ (Nordic Semiconductors). (B) Base station receiver. The receiver uses transceiver NRF24L01+ (Nordic Semiconductors), microcontroller STM32F4 (STMicroelectronics) and digital-to-analog converter DAC8568 (Texas Instruments).

2.3 Neural implant

Animal preparation. Two male rats (300 g, Rat A Sprague-Dawley, Rat B Long-Evans, Janvier, Le Genest-Saint-Isle, France) were anesthetized with equithesin (1 ml/300g) and placed in a stereotaxic apparatus. Anesthesia was maintained by supplemental doses when necessary. LFP oscillations were used to monitor anesthesia depth. Animals were placed on a heating pad to maintain constant body temperature. All experiments were performed in accordance with European Union Parliament and Council Directive 2010/63/UE regarding

the care and use of laboratory animals and recommendations of our institutional animal care and use committee (Agreement #: DR2014-41 and DR2015-46, CEEA-55 University Lyon 1).

Electrode implantation. After a local anesthetic injection (lidocaine, s.c.), the scalp was incised, and small burr holes were made in the skull above different structures whose coordinates are indicated in Table 1. Recordings were performed using either 80 μ m stainless steel or 45 μ m tungsten electrodes (see Table I). The electrodes were fixed with dental cement. A reference electrode was positioned in the skull bone above the contralateral

cortical hemisphere at 5 mm posterior to bregma (Rat A), or over the cerebellum (Rat B). All electrodes were connected to a nano-strip connector NSD-36-DD-GS (Omnetics) fixed onto the rat's head by dental cement. After a 2-week recovery period, the NeRD emitter was plugged on the rat's implant for recordings.

TABLE I
ELECTRODE IMPLANTATION IN RATS A AND B. THE STEREOTACTIC COORDINATES AND TYPE OF ELECTRODES ARE GIVEN FOR EACH STRUCTURE.

| Rat | Structure | Coordinates from bregma (mm) | electrode type |
|-----|---------------------------|------------------------------|-----------------------------|
| A | Olfactory bulb | +7.56 AP, 1 ML, 4 DV | monopolar, stainless steel, |
| A | Anterior piriform cortex | +2.76 AP, 3.5 ML, 6.6 DV | monopolar, stainless steel |
| A | Posterior piriform cortex | -2.4 AP, 5.5 ML, 8.0 DV | monopolar, stainless steel |
| A | Olfactory tubercle | +0.24 AP, 2.8 ML, 8.4 DV | monopolar, stainless steel |
| A | Striatum | +1.08 AP, 3.5 ML, 3.5 DV | monopolar, stainless steel |
| A | Hippocampus (CA1) | -3.8 AP, 2 ML, 2 DV | monopolar, stainless steel |
| A | Cerebellum | -12.24 AP, 3 ML, 2.5 DV | monopolar, stainless steel |
| B | Hippocampus (CA1) | -3.6 AP, 2.5ML, 3.1DV | 2 x monopolar, tungsten, |
| B | Hippocampus (DG) | -3.6 AP, 2.3ML, 3.6DV | monopolar, tungsten |
| B | Prelimbic cortex | +2.8, 0.7ML, 3.0DV | monopolar, tungsten |
| B | Anterior cingulate cortex | +2.8, 0.7ML, 4.2DV | monopolar, tungsten |
| B | Anterior piriform cortex | 4.2AP, 2.5ML, 5.2 DV | 2 x monopolar, tungsten |
| B | Orbitofrontal cortex | 4.2AP, 2.5ML, 4.2 DV | monopolar, tungsten |

3. RESULTS

3.1 Simulations

We first resort to computer simulations to assess how quantizer resolution and channel noise affect the signal-to-noise ratio (SNR) specified in units of decibels (dB)

$$SNR = 10 \log_{10} \sigma_{in}^2 / D_2$$

with σ_{in}^2 the input variance and D_2 the mean square error between original input and reconstructed output (Eq. 1 with $r = 2$). In numerical simulation, the original LFP signal is known exactly which makes possible to perform many reproducible trials with less constraint than with an implanted rat. Simulations were performed in Matlab based on six LFP signals previously recorded with NeRD in full resolution (16 bits) and rescaled in the unit interval.

Direct LFP quantization. Here we consider waveform coding by direct quantization of the LFP amplitude (Fig. 1B). An MOE quantizer is adapted on each sample according to Eqs. (4) and (6). Figure 4 shows the time course of a 2-bit quantizer (3 boundary points) during LFP encoding. We note that the MOE quantizer adapts to long-term drifts in baseline as well as sample-to-sample local variations. Performance is given in Fig. 5A. Increasing the number of bits by 1 improves the SNR by ~ 3 dB. For comparison, each additional bit to a fixed uniform quantizer yields an increase of ~ 6 dB, a result in line with the theory [17]. At 8 bits per sample, performance of fixed and adaptive quantizers are similar. Yet, at lower bitrates, the adaptive quantizer outperforms the fixed quantizer. At 2 bits per sample, the SNR of the adaptive quantizer is 20 dB higher than the one of the fixed quantizer. We further observe in Fig. 5B that adaptive quantization does not affect the power spectrum. The power spectrum displays a $1/f$ frequency scaling that is ubiquitous in electrophysiological recordings, irrespective of whether adaptive quantization is used or not. This result is important as fundamental frequencies in LFPs underlie neural processes. In Fig. 5B, the bump in the gamma band range reflects putative neural synchronization in the piriform cortex (see electrode implantation for NeRD in Table 1).

Differential LFP quantization. Quantization can also be part of a differential coding system (see Fig. 2). Here we consider quantizing the prediction error, that is, the difference between the LFP amplitude and a first-order prediction. An MOE quantizer is adapted on the prediction error according to Eqs. (4) and (6). Simulation results reveal that adaptive quantization outperforms fixed quantization at low bit rates (see Fig. 6A). When comparing Figs. 6A and 5A, we also note that differential quantization outperforms direct quantization. At 2 bit per sample, the prediction gain is ~ 10 dB, that is, SNR ~ 42 dB vs 32 dB for differential and direct adaptive quantization, respectively. Figure 6A also indicates the performance of adaptive differential pulse code modulation (ADPCM). The ADPCM implementation is based on application note AN643 from Microchip Technology and matlab code from MathWorks. Standard ADPCM uses a 4-bit uniform quantizer with adaptive step-size. We note that our adaptive differential quantizer at 4 bit per sample outperforms ADPCM by ~ 4 dB. This improvement is explained from the fact that, in our scheme, each boundary point is adapted independently whereas adaptation in ADPCM merely concerns the step size of a uniform quantizer. As a result, ADPCM can only cope with changes in the signal variance whereas our algorithm

can track any changes in signal pdf.

Noisy channel. We further tested whether our scheme is robust to channel noise. In NeRD, the data are transmitted as packets, each one containing 4 samples per channel. In case of a missing packet, the decoder thus fails to adapt to 4 consecutive samples. Figure 5B shows the SNR of a 2-bit quantizer (Eqs. 6 and 7) simulated in such noisy conditions. Without leakage parameter, that is $\beta = 0$ in Eq. (7), the SNR drops to 0 dB indicating that the quantization noise has same power than the original signal. Fortunately, the use of a leakage factor $\beta > 0$ in (7) allows to maintain an SNR above 30 dB over a range of noisy channels (up to 1% of missing packets).

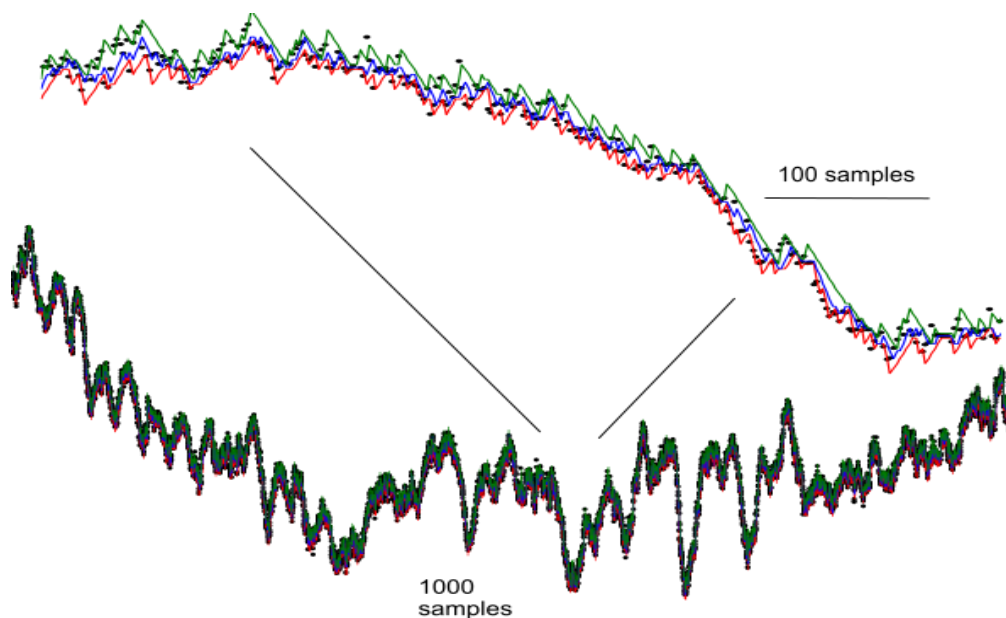


Fig. 4. Typical example of adaptive quantization of LFP signals. The LFP samples are indicated by black dots. The adaptive 2-bit quantizer is represented by three boundary points (red, blue and green curves). They evolve in time according to Eqs. (4) and (6) so as to track changes in the LFP.

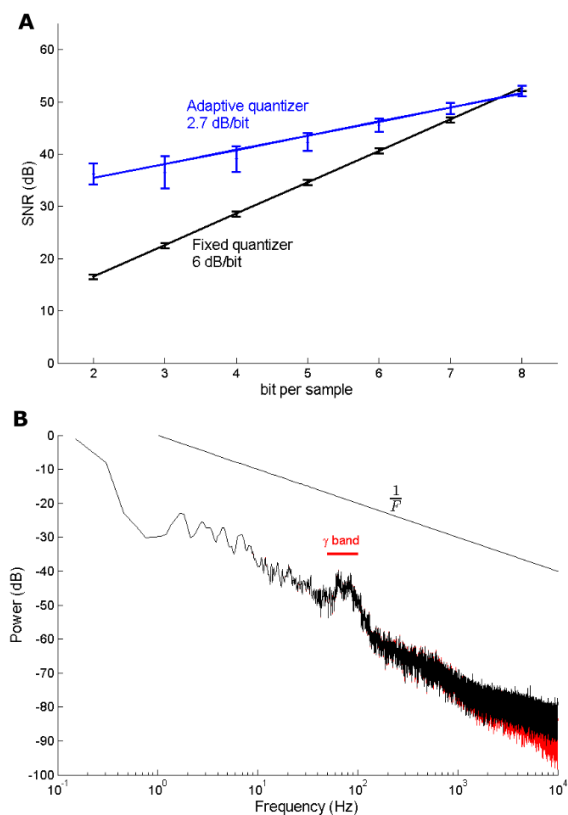


Fig. 5. Performance of direct LFP quantization. (A) SNR (in dB) as a function of quantizer resolution (bits/sample) for fixed and adaptive quantization. Data are presented as mean \pm s.d. (B) Representative example of LFP power spectrum. Original and quantized spectra are in red and black, respectively. They exhibit $1/f$ frequency scaling with a bump in the Gamma band typical of recordings in the rat's piriform cortex.

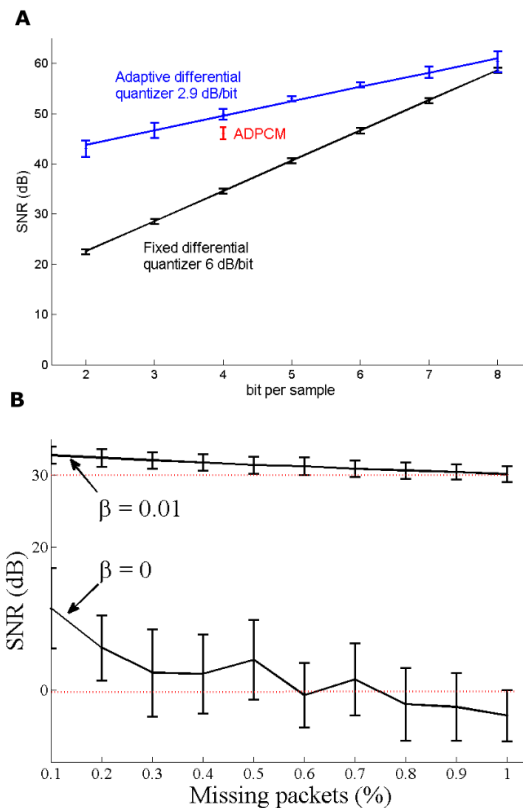


Fig. 6. Performance of differential LFP quantization. Data are presented as mean \pm s.d. (A) SNR (in dB) as a function of quantizer resolution (bits/sample) for n -bit fixed and adaptive quantization and 4-bit standard ADPCM. (B) SNR (in dB) obtained for a 2-bit adaptive quantizer with and without leakage factor β as a function of channel noise (percentage of missing packets).

3.2 Experiments with NeRD

Ex vivo experiments. We performed *ex vivo* experiments with NeRD to assess some characteristics of the device, such as the autonomy, transmission delay, packet loss and communication range. The autonomy of NeRD depends directly on the capacity of the battery and therefore on its weight. In our tests, NeRD was powered by a 100 mAh battery weighting 3.5 grams and providing approximately 2 hours and 40 mins of practical work within a communication range of 8 meters. The input-output delay in NeRD was found to be 4 ms. It is the same in all channels and does not depend on whether adaptive quantization is used or not. The rate of missing packets was evaluated as a function of the distance between the emitter and the receptor. A data loss occurs when the preamble or address of a packet is corrupted or when its CRC is invalid. At each distance considered, fifty thousand packets containing a unique identifier were sent and losses were detected from the missing identifiers. To estimate the variability, this procedure was repeated ten

times. The amount of losses increased significantly after 8 meters, thereby setting the maximal range of the system (Fig. 7A). From 1 to 8 meters the rate of missing packets was kept below 0.1%, partly because of the use of two transceiver modules in parallel. In order to evaluate the benefits of using two antennae, we estimated the error rates at a fixed distance of 3 m in the two configurations, with one and two transceivers. Fig. 7B indicates that the use of two transducers reduces the error rate more than twice on average. More important is the small variability obtained with two transducers so that the error rate can be kept small, *i.e.* below 0.1%, even in extreme trials where the communication channel is very noisy.

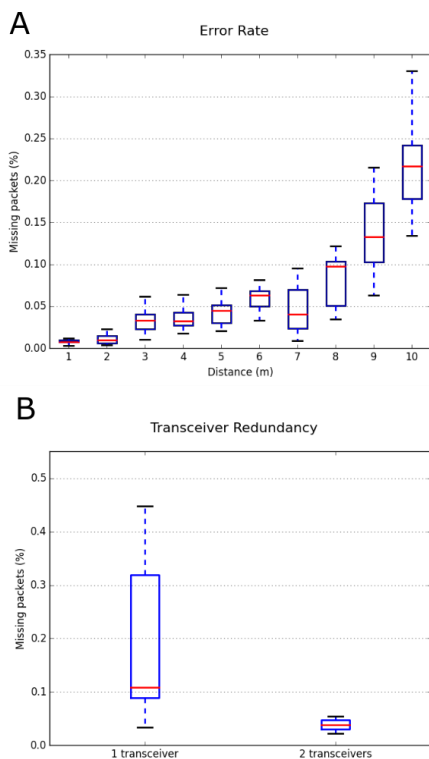


Fig. 7. In vitro experiments. Data losses during wireless transmission. (A) Loss rate as a function of the distance between emitter and receiver. (B) Loss rate with one and two transceivers (distance between emitter and receiver = 3 m).

In vivo experiments. NeRD was tested with freely moving rats (Fig. 8A). LFPs were recorded from stainless steel (Rat A) or tungsten (Rat B) electrodes. The results obtained are similar for the two preparations. The receiver was located at approximately one meter away and connected to a PC acquisition board via the DAC. Data were recorded and displayed online with the software OpenElectrophy [20]. Figure 8B (top panel) shows two LFPs simultaneously recorded in full resolution by two different electrodes. The spectrograms (Fig. 8B, bottom panel) clearly indicate the

presence of Gamma oscillations in the 50-80 Hz range (also revealed in the power spectrum of Fig. 5B). The second series of recordings was performed in the dorsal hippocampus. Fig. 8C (top panel) shows two signals corresponding to the same LFP recorded in full resolution (16-bit original) and compressed mode (2-bit quantization). The SNR between uncompressed and compressed LFPs is above 30 dB (33.2 ± 7.6 dB, mean \pm s.d., $n = 4$ recordings). Moreover, the presence of theta oscillations (4-6 Hz) that is ubiquitous in hippocampal recordings is independent on whether quantization is used or not (Fig. 8C, bottom panel).

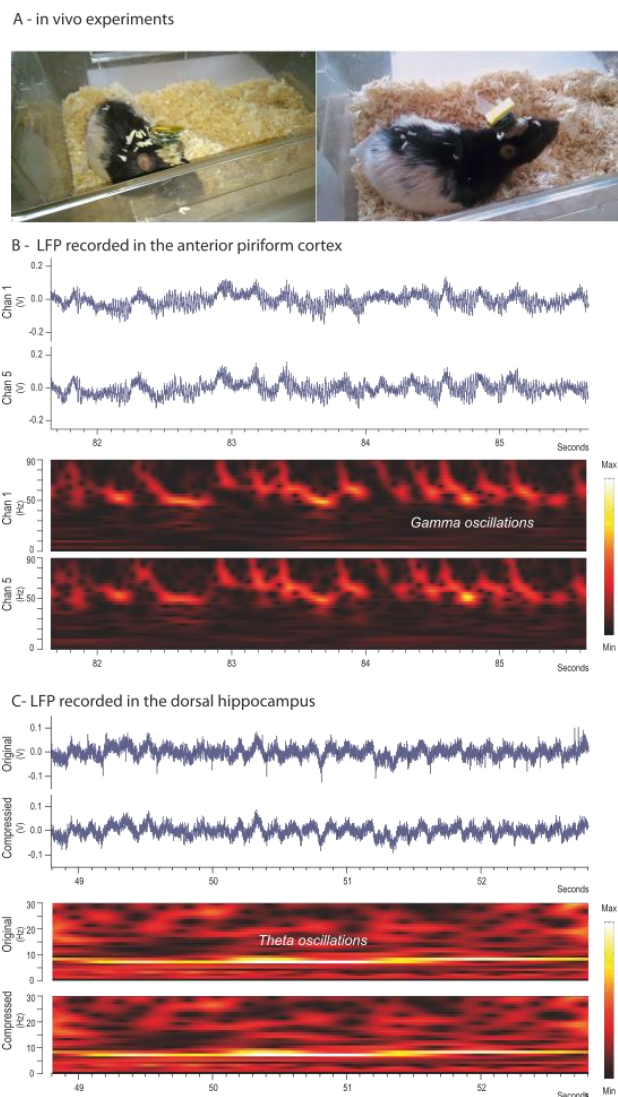


Fig. 8. In vivo experiments. (A) Freely moving rats carrying the NeRD emitter. (B) LFP recordings in the anterior piriform cortex. Top panel: two LFPs recorded in full resolution (16 bits) with two different electrodes. Bottom panel: the corresponding spectrograms reveal the presence of gamma oscillations. (C) LFP recordings in the dorsal hippocampus. Top panel: two LFPs recorded with the same electrode in both uncompressed

(16-bit full resolution) and compressed (2-bit quantization) modes. Bottom panel: the corresponding spectrograms reveal the presence of beta oscillations irrespective of the recording mode.

4. CONCLUSION

In recent years, the development of telemetry systems that record LFPs in moving animals and transmit them wirelessly to a remote computer have gained significant attention among the neuroscience community. Requirements for ecological recordings and animal welfare put strong constraints on device weight and power consumption. We argue that the use of adaptive non-uniform quantization is beneficial to decrease transmission bandwidth and thereby power consumption and battery weight. We proposed in this paper a backward adaptive algorithm that adapts the quantization intervals to changing statistics in the LFP. Its low computational complexity makes it suitable for hardware implementation with commercial microcontrollers.

As proof of concept, we developed NeRD, an open-source neural recording device whose schematics and firmware are available at <https://github.com/pseudoincorrect>. NeRD is a microcontroller-based telemetry system that consists of analog processing, adaptive non-uniform quantization and wireless transmission. With a weight of 8 grams including the battery (autonomy of 2h40), the NeRD prototype is readily mounted on a rat's head. The result of high SNR (above 30 dB) in recording LFPs (8 channels at 10 kHz) indicates that NeRD is a viable technique for bandwidth reduction (*i.e.* in this work from 1.28 Mb/sec in full resolution at 16 bits/sample to 160 Kb/sec in quantized mode at 2 bit/sample).

Future work will concentrate on increasing NeRD performance. One line of research that may prove beneficial in terms of SNR is to replace the fixed first-order predictor used in this work by an adaptive one. We note that backward adaptive prediction using a signed version of the least mean square algorithm [17] is possible for implementation simplicity in NeRD. Another point ought to be considered as future work is to increase the number of recording channels, sampling frequency and quantizer resolution. The current limitation is the microcontroller computational power that is too low to ensure adaptive quantization at $n > 2$ bits/sample over more than 8 channels. This problem could be solved by replacing or coupling the microcontroller with a logic programmable device. This way, adaptive quantization could be performed in parallel so that the performance

could grow up to 64 channels over $n > 2$ bits which corresponds to the transceiver bandwidth limit.

ACKNOWLEDGMENTS

This work acknowledges support from the French research program CPER Cyberentreprises (2015-2020), with participation from Région Lorraine and FEDER, and from the LABEX CORTEX (ANR-11-LABX-0042), within the program "Investissements d'Avenir" (ANR-11-IDEX-0007) operated by the French National Research Agency (ANR).

REFERENCES

- [1] R. E. Hampson, V. Collins, S. A. Deadwyler, "A wireless recording system that utilizes Bluetooth technology to transmit neural activity in freely moving animals," *J. Neurosci. Methods*, vol. 182, no. 2, pp. 195–204, 2009.
- [2] H. Miranda, V. Gilja, C. A. Chestek, K.V. Shenoy, T.H. Meng, "HermesD: A High-Rate Long-Range Wireless Transmission System for Simultaneous Multichannel Neural Recording Applications," *IEEE Trans. Biomedical Circuits & Systems*, vol. 4, no. 3, pp. 181–191, 2010.
- [3] D. A. Borton, M. Yin, J. Aceros, A. Nurmikko, "An Implantable Wireless Neural Interface for Recording Cortical Circuit Dynamics in Moving Primates," *J. Neural Eng.*, vol. 10, no. 2, pp. 026010, 2013.
- [4] M. Yin, D. A. Borton, J. Komar, N. Agha, Y. Lu, H. Li, J. Laurens, Y. Lang, Q. Li, C. Bull, L. Larson, D. Rosler, E. Bezaud, G. Courtine, A. V. Nurmikko, J. Aceros, A. Nurmikko, "Wireless neurosensor for full-spectrum electrophysiology recordings during free behavior," *Neuron*, vol. 84, no. 6, pp. 1170–82, 2014.
- [5] D. Ball, R. Kliese, F. Windels, C. Nolan, P. Stratton, P. Sah, J. Wiles, "Rodent Scope: A User-Configurable Digital Wireless Telemetry System for Freely Behaving Animals," *PLoS ONE*, doi: 10.1371/journal.pone.0089949, 2014.
- [6] R. R. Harrison, H. Fotowat, R. Chan, R. J. Kier, R. Olberg, A. Leonardo, F. Gabbiani, "Wireless Neural/EMG Telemetry Systems for Small Freely Moving Animals," *IEEE Trans. Biomedical Circuits and Systems. Neural Eng.*, vol. 5, no. 2, pp. 103–111, 2011.
- [7] T. A. Szuts, V. Fadeyev, S. Kachiguine, A. Sher, M. V. Grivich, M. Agrochão, P. Hottowy, W. Dabrowski, E. V. Lubenov, A. G. Siapas, N. Uchida, A. M. Litke, M. Meister, "A wireless multi-channel neural amplifier for freely moving animals," *Nature neuroscience*, vol. 14, pp. 263–269, 2011.
- [8] S. Roy, X. Wang, "Wireless multi-channel single unit recording in freely moving and vocalizing primates," *J. Neuroscience Methods*, vol. 203, pp. 28–40, 2012.
- [9] B. Gosselin, A. E. Ayoub, J. F. Roy, M. Sawan, F. Lepore, A. Chaudhuri, D. Guitton, "A mixed-signal multichip neural recording interface with bandwidth reduction," *IEEE Trans. Bio. Circ. Syst.*, vol. 3, no. 3, pp. 129–141, 2009.
- [10] A. Bonfanti, G. Zambra, G. Baranauskas, G. N. Angotzi, E. Maggiolini, M. Semprini, A. Vato, L. Fadiga, A. S.

- Spinellia, A. L. Lacaita, "A wireless microsystem with digital data compression for neural spike recording," *Microelectronic Engineering*, vol. 88, pp. 1672–1675, 2011.
- [11] H. Hosseini-Nejad, A. Jannesari, A. M. Sodagar, "Data Compression Based on Discrete Cosine Transform for Implantable Neural Recording Microsystems," *IEEE Conference on Circuit and Systems (ICCAS)*, Kuala Lumpur, Malaysia, 2012.
- [12] K. G. Oweiss, A. Mason, Y. Suhail, A. M. Kamboh, K. E. Thomson, "A Scalable Wavelet Transform VLSI Architecture for Real-Time Signal Processing in High-Density Intra-Cortical Implants," *IEEE Trans. Circuits and Systems*, vol. 54, no. 6, pp. 1266-1278, 2007.
- [13] S. Mukhopadhyay, G.C. Ray, "A new interpretation of nonlinear energy operator and its efficacy in spike detection" *IEEE Trans. Biomedical Engineering*, vol. 45, no. 2, pp. 180-187, 1998.
- [14] I. Obeid, P.D. Wolf, "Evaluation of spike-detection algorithms for a brain-machine interface application" *IEEE Trans. Biomedical Engineering*, vol. 51, no. 6, pp. 905-911, 2004.
- [15] S. Gibson, J.W. Judy, D. Marković, "Technology-aware algorithm design for neural spike detection, feature extraction, and dimensionality reduction" *IEEE Trans Neural Syst Rehabil Eng.*, vol. 18, no. 5, pp. 469-478, 2010.
- [16] S. Kassan, "Quantization based on the mean absolute error criterion", *IEEE Trans. Commun.*, vol. 26, no. 2, pp. 267-270, 1978.
- [17] N. S. Jayant, P. Noll, *Digital Coding of Waveforms*. Prentice-Hall, 1984.
- [18] P.F. Panter, W. Dite, "Quantization distortion in pulse-count modulation with nonuniform spacing of levels," *Proc. IRE*, vol 39, pp. 44-48, 1951.
- [19] D. Martinez, M. M. Van Hulle, "Generalized Boundary Adaptation Rule for minimizing r -th power law distortion in high resolution quantization," *Neural Networks*, vol. 8, no. 6, pp. 891-900, 1995.
- [20] D.G. Messerschmitt, "Quantizing for maximum output entropy," *IEEE Trans. Information Theory*, vol. 17, no. 5, pp. 612, 1971.
- [21] M. M. Van Hulle, D. Martinez, "On an unsupervised learning rule for scalar quantization following the maximum entropy principle," *Neural Computation*, Vol. 5, no. 6, pp. 939-953, 1993.
- [22] M. M. Van Hulle, D. Martinez, "On a novel unsupervised competitive learning algorithm for scalar quantization," *IEEE Transactions on Neural Networks*, vol. 5, no. 3, pp. 498-501, 1994.
- [23] D. Martinez, W. Yang, "A robust backward adaptive quantizer" in *IEEE Workshop on Neural Networks for Signal Processing*, vol. 5, pp. 531-540, 1995.
- [24] S. Garcia, N. Fourcaud-Trocmé, "OpenElectrophy: An Electrophysiological Data- and Analysis-Sharing Framework," *Frontiers in neuroinformatics*, vol. 3, no. 14, 2009.